Ewing sarcoma inhibition by disruption of EWSR1-FLI1 transcriptional activity and reactivation of p53

Ent, W. van der; Jochemsen, A.G.; Teunisse, A.F.; Krens, S.G.; Szuhai, K.; Spaink, H.P.; ... ; Snaar-Jagalska, B.E.

Journal of Pathology
J Pathol 2014; **233:** 415–424
Published online 27 June 2014 in Wiley Online Library (wileyonlinelibrary.com) DOI: 10.1002/path.4378

ORIGINAL PAPER

Ewing sarcoma inhibition by disruption of EWSR1–FLI1 transcriptional activity and reactivation of p53

Wietske van der Ent,[1,2] Aart G Jochemsen,[3] Amina FAS Teunisse,[3] SF Gabriel Krens,[1] Karoly Szuhai,[3] Herman P Spaink,[1] Pancras CW Hogendoorn[2*] and B Ewa Snaar-Jagalska[1*]

[1] *Institute of Biology, Leiden University, The Netherlands*
[2] *Department of Pathology, Leiden University Medical Center, The Netherlands*
[3] *Department of Molecular Cell Biology, Leiden University Medical Center, The Netherlands*

**Correspondence to: PCW Hogendoorn, Albinusdreef 2, 2333 ZA Leiden, The Netherlands. E-mail: p.c.w.hogendoorn@lumc.nl*
Or BE Snaar-Jagalska, Einsteinweg 55, 2333 CC Leiden, The Netherlands. Email: b.e.snaar-jagalska@biology.leidenuniv.nl

Abstract

Translocations involving ETS-transcription factors, most commonly leading to the EWSR1–FLI1 fusion protein, are the hallmark of Ewing sarcoma. Despite knowledge of this driving molecular event, an effective therapeutic strategy is lacking. To test potential treatment regimes, we established a novel Ewing sarcoma zebrafish engraftment model allowing time-effective, dynamic quantification of Ewing sarcoma progression and tumour burden *in vivo*, applicable for screening of single and combined compounds. In Ewing sarcoma the tumour-suppressor gene *TP53* is commonly found to be wild-type, thus providing an attractive target for treatment. Here, we study *TP53* wild-type (EW7, CADO-ES1 and TC32) and *TP53*-deleted (SK-N-MC) Ewing sarcoma cell lines to investigate the potentiating effect of p53 reactivation by Nutlin-3 on treatment with YK-4-279 to block transcriptional activity of EWSR1–FLI1 protein. Blocking EWSR1–FLI1 transcriptional activity reduced Ewing sarcoma tumour cell burden irrespective of *TP53* status. We show that simultaneous YK-4-279 treatment with Nutlin-3 to stabilize p53 resulted in an additive inhibition of *TP53* wild-type Ewing sarcoma cell burden, whilst not affecting *TP53*-deleted Ewing sarcoma cells. Improved inhibition of proliferation and migration by combinatorial treatment was confirmed *in vivo* by zebrafish engraftments. Mechanistically, both compounds together additively induced apoptosis of tumour cells *in vivo* by engaging distinct pathways. We propose reactivation of the p53 pathway in combination with complementary targeted therapy by EWSR1–FLI1 transcriptional activity disruption as a valuable strategy against p53 wild-type Ewing sarcoma.

Keywords: Ewing sarcoma; drug synergism; p53; tumour growth; zebrafish; anti-cancer drug screen; molecular targeted therapy

Received 24 December 2013; Revised 14 May 2014; Accepted 18 May 2014

No conflicts of interest were declared.

Introduction

Ewing sarcoma (EWS) is the second most common sarcoma of bone in children and young adults [1]. Transformation is believed to be caused by a chromosomal translocation fusing the *EWSR1* gene to a member of the ETS transcription factor family of genes, resulting in a highly deregulated transcription factor [2]. The two most common gene fusions are *EWSR1–FLI1* (85% of cases) and *EWSR1–ERG* (10% of cases) [3,4]. Around 25% of patients have metastases present at the time of diagnosis [5]. Currently, these patients have a 2 year event-free survival of ~20% [6] and a satisfactory treatment regime is lacking. Inactivation of the transcriptional activity of EWSR1–ETS oncogene, in combination with reactivation of p53, which is wild-type in ~90% of these tumours, could provide a potential treatment strategy [7]. To test this hypothesis, two potential drugs operating via a different mode of action were used in this study: Nutlin-3 [8], a p53 activator, and YK-4-279, a small compound inhibiting the interaction between EWSR1–ETS protein and RNA helicase A and thereby inhibiting its gene-transactivating function [9]. Individually, these compounds are known to modulate EWS tumour growth. Treatment with YK-4-279 elicited a marked reduction of EWS tumour growth in mouse xenografts [9], and reactivation of the p53 pathway by Nutlin-3 induced an apoptotic response of EWS cell lines *in vitro* [10]. Here we show how the combination of these compounds affects EWS tumour behaviour, both in culture and in a newly-established zebrafish xenotransplantation model.

The zebrafish (*Danio rerio*) is increasingly used as a model organism to study cancer [11]. Benefits include large clutch size, *ex utero* development, temporal separation between innate and adaptive immunity, transparency and easy manipulability of embryos [12]. There is high conservation of oncogenes and tumour-suppressor genes between zebrafish and human [13] and various oncogenic transgenic zebrafish lines

have been developed [14]. The histology of zebrafish tumours has been shown to be highly similar to tumours found in human cancers [15]. The adaptive immune system in zebrafish does not reach maturity until 4 weeks post-fertilization [16], allowing circumvention of cell graft–host rejection by using zebrafish in early stages.

Zebrafish embryos can absorb various small molecular weight compounds from water, which is advantageous when screening for anti-cancer compounds [17–21]. Use of transgenic lines with fluorescent vasculature or neutrophil granulocytes [22,23] allows live imaging of cancer development and interaction with the microenvironment *in vivo* within 1 week.

We established a zebrafish model for EWS development, applicable for real-time *in vivo* monitoring of tumour progression at single-cell level, by recording the induction of angiogenesis, EWS proliferation and migration, as well as tumour cell interaction with the host immune system. The model was utilized to investigate combinatorial treatments with multiple drugs. Such multi-hit approaches have until now been limited in test animals due to lack of throughput.

In this paper we show both in culture and *in vivo* that p53 stabilization by Nutlin-3 has an additive effect on the ability of YK-4-279 to reduce tumour burden via EWSR1–ETS transcriptional deactivation. Both compounds caused tumour cell apoptosis *in vivo* via distinct pathways. We propose that p53 reactivation in combination with targeted EWSR1–ETS transcriptional deregulation as an attractive therapeutic strategy for patients with p53-wild-type Ewing sarcoma.

Materials and methods

Cell culture

Ewing sarcoma cell lines (CADO-ES, EW3, EW7, L1062, TC32, TC71 and SK-N-MC) were present at the Leiden University Medical Centre and authenticated by Promega Powerplex assay. Cells were cultured in Iscove's Modified Dulbecco's Medium (IMDM; Life Technologies) with 10% fetal bovine serum (FBS; Life Technologies) at 37 °C and 5% CO_2. Stably fluorescent lines were produced by transduction with mCherry-expressing lentiviral vectors (kindly provided by Professor Dr Hoeben, Leiden University Medical Centre). Non-fluorescent lines were labelled using Celltracker CM-DiI (Life Technologies) according to the manufacturer's instructions.

Zebrafish maintenance

ABTL, Albino, Casper, *TG(fli1:EGFP)*, *TG(mpo:GFP)i114* and *tp53*^{M214K} zebrafish lines were handled in compliance with local animal welfare regulations and maintained according to standard protocols (www.ZFIN.org). Animal experiments were approved by the Animal Care Committee of the Faculty of Medicine, Leiden University (Approval No. UDEC10027).

Tumour cell implantation

Embryos or 35 days post-fertilisation (dpf) juveniles were anaesthetized with 0.001% tricaine (Sigma-Aldrich). Single-cell suspension in 2% polyvinylpyrrolidone-40 (Sigma-Aldrich) was loaded into 1.0 mm o.d. × 0.78 mm i.d. borosilicate needles (Harvard Apparatus); 500–800 cells were injected into the yolk or eye, using a Pneumatic PicoPump (World Precision Instruments; 10–20 psi, 100–400 ms). The larvae were maintained at 34 °C. For 35 dpf juveniles, the water temperature was raised from 28 °C to 34 °C over the course of a week prior to implantation. Juveniles were immunosuppressed by the addition of 10 µg/ml dexamethazone (Sigma-Aldrich) to the water, refreshed every other day, starting 2 days before implantation [24].

In vivo toxicity test of chemical compounds and analysis

Racemic (±) Nutlin-3 (Cayman Chemical, USA) and racemic YK-4-279 (kindly provided by Dr Toretsky) stock solutions were dissolved to a concentration of 1 mM in DMSO. Six embryos were placed in each well of a 24-well plate in a volume of 1 ml Instant Ocean egg water supplemented with chemical compounds, with daily refreshing of the solutions. The embryos were fixed overnight (O/N) in 4% paraformaldehyde (PFA) at 4 °C, and imaged in glass-bottomed 96-well plates using a NIKON3 confocal microscope (×4 lens). Image processing was performed using ImageJ 1.43 (National Institutes of Health, USA). ImagePro Analyser 7.0 (Media Cybernetics) analysis was performed as described previously [25].

Proliferation assay in cell culture

For measurement of relative EWS cell survival of each treatment, 3000 or 5000 cells/well were seeded in triplicate in full medium in a 96-well microtitre plate. Next day, the medium was replaced with medium containing the indicated compounds or vehicle concentrations. After indicated times, relative growth was measured using a WST-1-based colourimetric assay (Roche Diagnostics), according to the manufacturer's instructions. For synergy studies, effects were calculated as 'affected fraction' of treated versus untreated cells, according to the method of Chou [26]. Dose–effect analyses were performed using CompuSyn software (Compusyn).

Western blotting

Western blots were performed as described previously [27]. Gels were loaded with 10–15 µg total protein lysates. The following antibodies were used: anti-p53 (DO-1, 1:500; Santa Cruz Biotechnology), anti-HDM2 (SMP14, 1:500; Santa Cruz Biotechnology), anti-HDMX (rabbit polyclonal A300-287A, 1:2000; Bethyl Laboratories) or mouse monoclonal 8C6 (1:1000; Millipore), anti-p21 (CP74, 1:500; Upstate

Biotechnology), anti-PARP (cat. no. 9542, 1:1000; Cell Signaling Technology) and anti-Vinculin (hVIN1, 1:1000; Sigma-Aldrich).

Immunohistochemistry and TUNEL staining

Whole-mount zebrafish immunohistochemistry was performed as described previously [28]. The following antibodies were used: CD99-O13 (Covance); L-plastin (kindly provided by Dr A. Huttenlocher); AlexaFluor 488 and 568 (Life Technologies). TUNEL staining was performed using an ApopTag Peroxidase *In Situ* Apoptosis Detection Kit (Merck–Millipore) and TSA-Plus Fluorescein system (Perkin-Elmer). For staining of tissue sections, embryos were fixed in 4% PFA, embedded in paraffin, cut into 4 µm sections and stained with haematoxylin and eosin (H&E), CD99-O13 and periodic acid–Schiff (PAS). Quantification of apoptosis was performed by counting TUNEL-positive versus TUNEL-negative cells for four or more embryos/condition, and noted in the text as mean percentage apoptotic cells ± standard error of the mean (SEM).

Statistical analysis

A one-way ANOVA test with a Dunnet's post-test was utilized to determine the *in vivo* drug treatment effects. All statistical tests were two-sided. Values were expressed as means with 95% confidence intervals (CIs). *$p < 0.05$ was considered statistically significant; **smaller values (**$p < 0.01$). Statistical analyses were performed using GraphPad Prism v 4.

Results

Characterization of the behaviour of EWS cells within the zebrafish xenotransplantation model

Previous reports have shown that zebrafish can be used as a host organism to study the progression of various types of cancer, using either transgenic or xenograft models [11]. To determine whether zebrafish is a suitable model organism for Ewing sarcoma progression, a panel of EWS cell lines was implanted in the yolk of 2 dpf embryos (Figure 1A–C).

Cell lines derived from metastatic and primary tumours were selected for different translocation types and status of the p53 pathway (Table 1). Induction of angiogenesis was scored 24 h post-implantation (hpi; Figure 1D–F), as described by Nicoli and Presta [34] and Nicoli *et al* [35]. Implanted cell lines differed in potential to induce angiogenesis, ranging from angiogenesis observed in 25% of fish (EW3, $n = 52$), to no observed angiogenesis (CADO-ES, $n = 31$). To ensure specificity of the angiogenic response by implanted cells and to exclude a response to injection-induced wounding, zebrafish fibroblast cells and cancer cells that had undergone several freeze–thaw cycles were implanted.

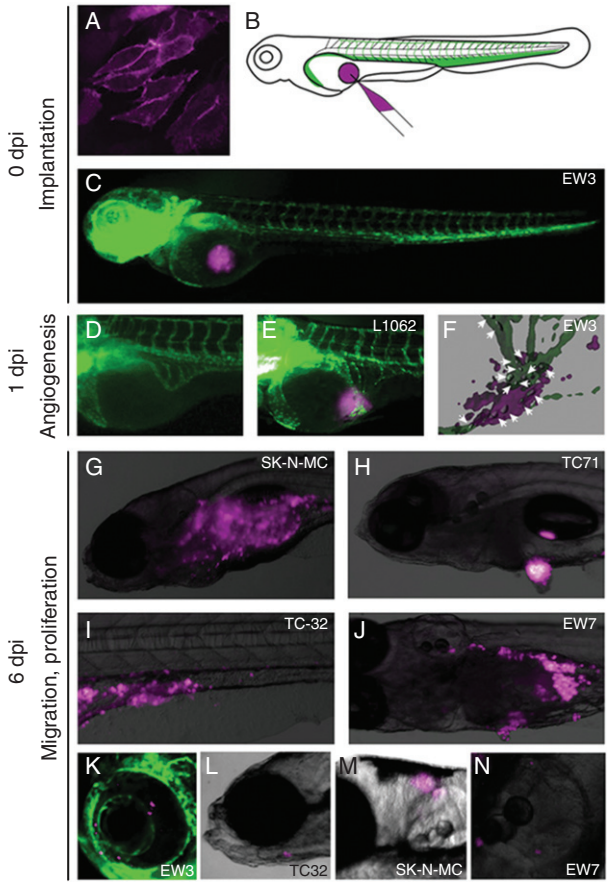

Figure 1. Workflow of xenotransplantation experiment. (A) Cells stably expressing mCherry or labelled with fluorescent membrane marker. (B) Schematic view of injection in a 2 dpf embryo; magenta, EWS cells; green, vasculature of tail and yolk. (C) *TG(fli1:EGFP)* 2 dpf embryo with green vasculature [22], injected with EWS cells (magenta) 3 h after implantation. (D) Regular development of the subintestinal vein complex of an uninjected 3 dpf *TG(fli1:EGFP)* embryo. (E) Angiogenic sprouting of vessels from the subintestinal vein complex induced by the implanted EWS cells in *TG(fli1:EGFP)* embryo, 1 dpi. (F) Interaction (white arrows) between implanted EWS cells and vasculature of *TG(fli1:EGFP)* embryo, 1 dpi. (G–J) Proliferation, outgrowth and migration to head of ABTL embryo implanted with EWS cells, 6 dpi. (K) Migration to eye. (L) Migration to jaw. (M) Migration to brain. (N) Migration to otic vesicle. Data are representative images of > 10 independent, highly reproducible experiments

Neither zebrafish cells nor cell fragments were able to elicit an angiogenic response (see supplementary material, Figure S1, $n \geq 35$).

Haematogenous dissemination of all tested cell lines was observed to fins, head and body (Figure 1G–N, Table 1) of the zebrafish larvae within 6 dpi. In addition, some cell lines (TC32, TC71, EW7) were capable of forming tumour cell outgrowths, primarily in the proximity of the abdomen (Figure 1H). Proliferation of cells was scored by the amount of red fluorescent signal/larva. At 6 dpi, a variation in the amount of cell burden could be observed for different cell lines. All tested cell lines proliferate and migrate within the embryo and most EWS cells showed the ability to induce an angiogenic response (Table 1), independent of translocation

Table 1. Overview of EWS cell properties

Cell line	Primary or metastasis	Translocation	*TP53* status	Behaviour in zebrafish embryonic xenograft		
				Tumour burden	Migration (95% CI)	Angiogenesis
CADO-ES [29]	Metastasis	*EWSR1-ERG*	Wild-type	Medium	48.5–86.1	No
EW3 [29]	Primary	*EWSR1-ERG*	Wild-type	Low	57.2–70.8	Yes
EW7 [29]	Primary	*EWSR1-FLI1*	Wild-type	Medium	74.8–78.6	Yes
L1062 [30]	Primary	*EWSR1-FLI1*	Mutant	High	37.7–62.3	Yes
SK-N-MC [31]	Metastasis	*EWSR1-FLI1*	Deletion	High	61.1–92.3	Yes
TC71 [32]	Recurrent	*EWSR1-FLI1*	Mutant	Medium	69.5–73.3	Not analysed
TC32 [33]	Metastasis	*EWSR1-FLI1*	Wild-type	Medium	56.7–64.5	Yes

Tumour burden is classified according to the following definitions: High, high tumour cell burden in > 80% of larvae; Medium, high tumour cell burden in 50–80% of larvae; Low, minimal amounts of tumour cells in > 50% of larvae.
Migration is represented as the percentage of embryos which showed cells migrating away from the site of implantation.
All xenograft data were collected from three or more individual experiments, with $n > 30$, and no more than 80% lethality/group.

type or *TP53* status, with EW7 having the most potent tumour progression properties.

Migration of EWS cell within the zebrafish host

EWS cells showed strong metastatic capacities in the zebrafish larvae. Further analysis on engrafted larvae was performed to obtain insight into the migration mechanism.

High-magnification imaging at sites of dissemination revealed that EWS cells resided both inside and outside the blood vessels (Figure 2A, B), suggesting a role of the circulatory system in their migration. Immunohistochemistry demonstrated that migratory cells were positive for EWS markers (CD99, PAS; Figure 2C; see also supplementary material, Figure S2), thus retaining EWS properties *in vivo*.

Major organ systems are still in development in zebrafish larvae. To determine whether EWS cells could home to specific organs, cells were implanted via vessels in the eye into the bloodstream of fully-developed 35 dpf Casper zebrafish juveniles lacking melanocytes and iridiophores [36], enabling non-invasive late-stage microscopy. Cells were observed in the abdomen of the zebrafish at 6 dpi, using live stereo imaging. Immunohistochemical analysis at 6 dpi showed cells in the gut and kidney of the larvae (see supplementary material, Figure S3; $n = 12$), proving that migration of EWS in embryos resembles metastatic behaviour in adult zebrafish stages.

To exclude false-positive results for migration due to cell debris taken up and transported by embryonic leukocytes (primarily neutrophils and macrophages at this stage of development), cells were implanted into embryos expressing GFP in the neutrophils [23]. Neutrophils and various EWS cells were shown to interact (Figure 2E, F) but uptake of EWS cell material by neutrophils was not observed.

At the time of the experiment, transgenic embryos with fluorescent macrophages were not yet available. To examine whether macrophages played a role in migration, leukocytes were detected by whole-mount immunohistochemistry against L-plastin (a zebrafish pan-leukocyte marker). Co-localization of L-plastin and red fluorescent cells showed that some, but not all, EWS cells in the bodies of the larvae were taken up by leukocytes (Figure 2G, H), suggesting that EWS cells disseminate mainly due to active migration. No neutrophil uptake was observed in previous experiments, indicating that macrophages are responsible for the observed partial phagocytosis of EWS cells.

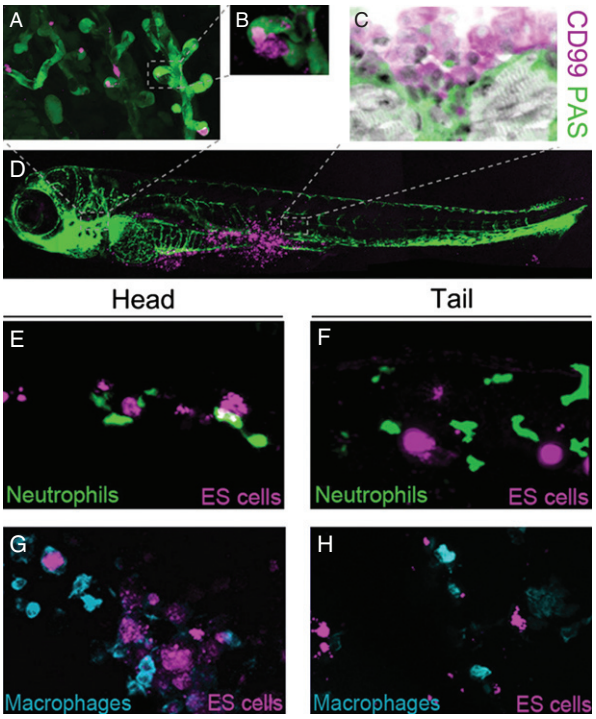

Figure 2. Behaviour of EWS cells within embryo host. (A) EWS cells (magenta) inside and next to blood vessels in the gills of *TG(fli1:EGFP)* embryo, 5 dpi. (B) Detail of (A), showing cells within the lumen of the blood vessel. (C) Paraffin section of 5 dpi embryo with CD-99-positive EWS cells (magenta) in the muscle: grey, H&E; magenta, CD99; green, PAS. (D) Confocal overview image of *TG(fli1:EGFP)* embryo with EWS cells spreading to the head, muscles and fins, 5 dpi. (E) *TG(mpx:GFP)i114* embryo showing EWS cells (magenta) interacting with neutrophils (green), 5 dpi, head. (F) *TG(mpx:GFP)i114* embryo showing EWS cells (magenta) interacting with neutrophils (green), 5 dpi, tail. (G) ABTL embryo showing EWS cells (magenta) interacting with macrophages (blue), 5 dpi, head. (H) ABTL embryo showing EWS cells (magenta) interacting with macrophages (blue), 5 dpi, tail. Data are representative images of > 10 independent, reproducible experiments (each $n > 30$)

Effect of Nutlin-3 and YK-4-279 on *TP53* wild-type and *TP53*-deletion EWS cell lines

In ~90% of EWS tumours, *TP53* is found to be wild-type [7], providing an interesting target for treatment strategies. Previous reports showed Nutlin-3 to have an adverse effect on the malignant potential of EWS cells [37] via the stabilization of the p53 protein and subsequent apoptotic pathway activation. Nevertheless, single-compound treatments may allow the escape of non-respondent cells, which can be reduced by simultaneously adding drugs with a different target. For this purpose, we used YK-4-279, a small molecule reported to disrupt EWS–FLI1 transcriptional activity by blocking the interaction between RNA helicase A and EWS–FLI1 protein [9].

We tested the sensitivity of *TP53* wild-type EW7, CADO-ES1 and TC32 and *TP53*-deletion SK-N-MC cell lines in culture for various concentrations of Nutlin-3 or YK-4-279, or a combination of both, by comparing the relative growth of the cells after 72 h of treatment.

Nutlin-3 reduced the growth of EW7 in a dose-dependent manner ($EC_{50} = 0.97\,\mu M$; Figure 3A), as well as CADO-ES1 and TC32 (see supplementary material, Figure S4). SK-N-MC cells, which lack a full-length p53 protein, were essentially not affected by Nutlin-3 treatment ($EC_{50} > 100\,\mu M$; Figure 3B). YK-4-279 reduced the growth of all four cell lines, with SK-N-MC appearing slightly more sensitive than EW7 ($EC_{50} = 0.46$ and $0.65\,\mu M$, respectively; Figure 3A, B; see also supplementary material, Figure S4). The combination of Nutlin-3 and YK-4-279 was found to have a synergistic inhibitory effect on the growth of EW7, CADO-ES1 and TC32 but not on SK-N-MC (Figure 3A, B; see also supplementary material, Figure S4).

Cell culture experiments confirmed that, as Nutlin-3 works largely in a p53-dependent and YK-4-279 mainly in a p53-independent manner, cell lines with a differential p53 expression have dissimilar responses to the applied compounds.

Effect of Nutlin-3 and YK-4-279 on *TP53* wild-type and mutant zebrafish

Immersion is a well-established method for drug treatment of zebrafish larvae [12,38]. To determine whether our xenotransplantation model was suitable for drug testing, Nutlin-3 and YK-4-279 were applied to embryos injected with EWS cells.

As pathways concerned with cancer can be involved in larval development, we initially performed toxicity tests on mock-injected larvae. For both compounds, a concentration of 2 μM had a strong inhibitory effect in culture but allowed sufficient survival *in vivo* (Figure 3C). No significant difference in lethality was observed when compounds were applied to *tp53*^{M214K} mutant zebrafish (Figure 3D), excluding a lethal effect of Nutlin-3 by

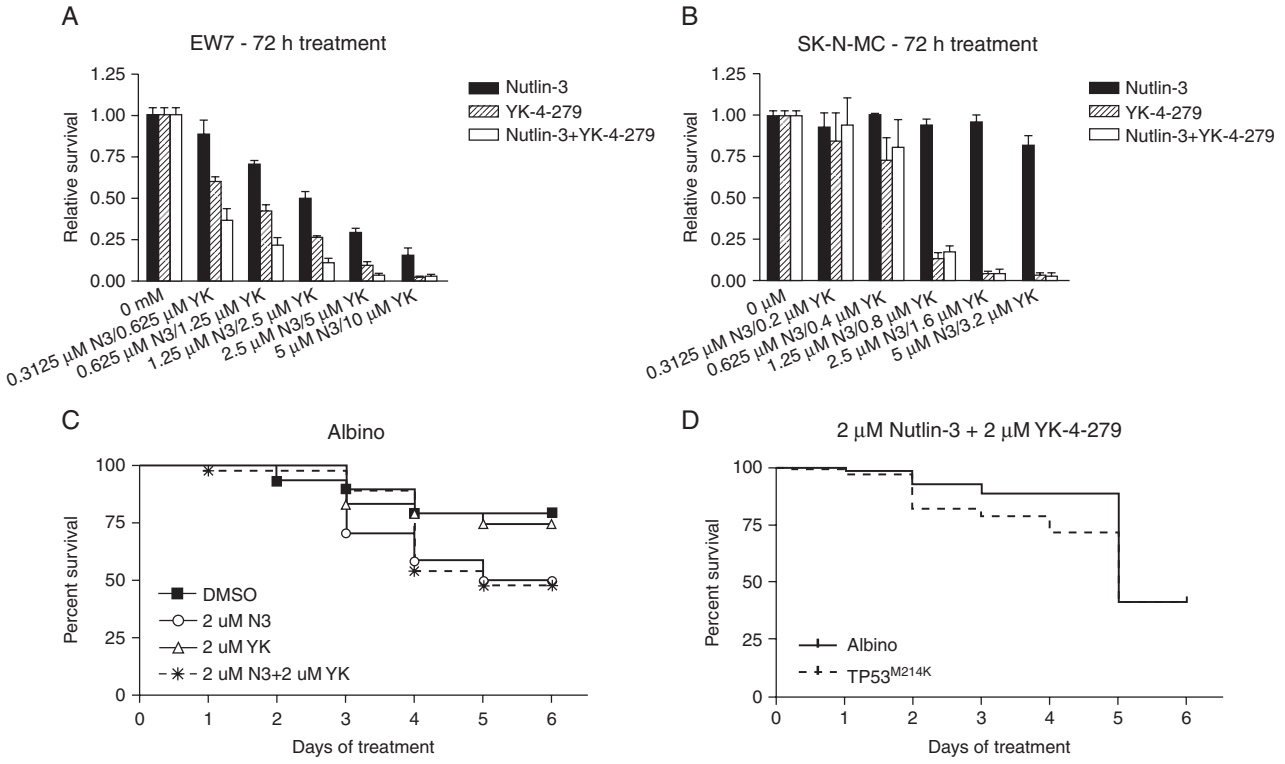

Figure 3. The effect of Nutlin-3 and YK-4-279 on EWS cells in culture and zebrafish embryos. (A) WST-1 assay for measuring relative survival of EW7 cells treated for 72 h with Nutlin-3 (EC-50: 0.97 μM), YK-4-279 (EC-50: 0.65 μM) or a combination thereof. All measurements were performed in triplicate; error bars represent 95% confidence interval (CI). (B) WST-1 assay for measuring relative survival of SK-N-MC cells treated for 72 h with Nutlin-3 (EC-50, > 100 μM), YK-4-279 (EC-50, 0.46 μM) or a combination thereof. All measurements were performed in triplicate; error bars represent 95% CI. (C) Toxicity test of compounds on albino embryos treated from 2 dpf onwards; $n \geq 24$/condition. (D) Effect of treatment on albino embryos compared to *tp53*^{M214K} embryos treated from 2 dpf onwards; $n = 72$/condition

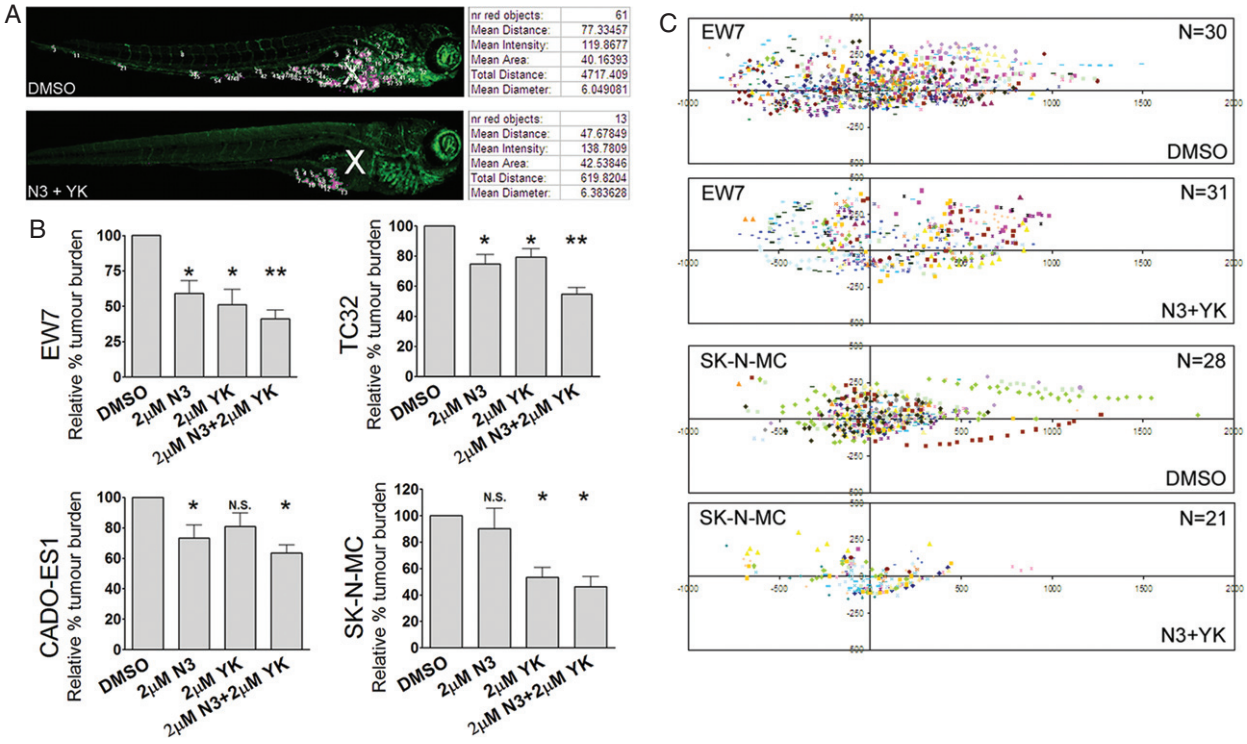

Figure 4. The effect of Nutlin-3 and YK-4-279 on EWS cells *in vivo*. (A) Quantitative analysis [25] of embryos implanted with SK-N-MC cells, treated with DMSO or Nutlin-3 and YK-4-279. Algorithms use the green channel to find the outline of the *TG(fli1:EGFP)* embryo and estimate the site of implantation (white X). Using the mCherry signal from EWS cells, all tumour cell foci (objects) are outlined and numbered. To determine tumour burden/embryo, number of objects was multiplied by the average size of objects. Migration away from the site of implantation was determined per object and represented in scatter dot-plots. (B) Tumour burden of EWS cells in embryos, 6 dpi, normalized against DMSO. Differences between means were obtained by one-way analysis of variance (ANOVA) with a Dunnett's post-test; $^{*}p < 0.05$; $^{**}p < 0.01$; N.S., no significant difference; error bars represent 95% confidence interval. (C) Scatter dot-plot for migration; each colour represents one embryo/group, each dot one cluster of tumour cells. Site of implantation, X, Y = 0, 0

activation of wild-type zebrafish p53. In addition to stabilizing p53, Nutlin-3 may also up-regulate TAp73 levels [39,40]. This protein plays an important role in the embryonic development of zebrafish and may be responsible for the higher toxicity of Nutlin-3 in these experiments [41]. At concentrations of 4 μM, both Nutlin-3 and YK-4-279 caused > 40% lethality (see supplementary material, Figure S5), so further experiments were performed, with concentrations of 2 μM, in p53 wild-type zebrafish, to simulate the typical microenvironment as closely as possible.

Effect of Nutlin-3 and YK-4-279 on EWS cells in the xenotransplantation model

After implantation with EW7 and SK-N-MC cells in larvae, treatment with Nutlin-3, YK-4-279 or a combination thereof, was started 24 hpi. At 6 dpi, quantitative analysis was performed on confocal images, providing information on the amount, size and migration of tumour cell foci for each embryo (Figure 4A shows two examples of the read-out). Mean reduction of tumour burden (MR), as obtained by the cumulative area of tumour foci, and 95% CI were determined for each group compared with DMSO controls. Our quantification revealed that larvae treated with both Nutlin-3 and YK-4-279 showed a significantly reduced growth of EW7 (MR 41%, CI 1–81%, $p < 0.05$; and MR 48%, CI 8–88%, $p < 0.05$, respectively), as well as CADO-ES1 and TC32 (Figure 4B). The combination of compounds had an additive effect on this decrease of wild-type EWS growth (EW7: MR 61.6%, CI 22.7–100%, $p < 0.01$). The growth of SK-N-MC was significantly reduced in embryos treated with YK-4-279 (MR 46.6%, CI 7.3–85.9%, $p < 0.05$) but not by Nutlin-3, and minimal additive effects were observed for double treatment (MR 53.8%, CI 10.0–97.6%, $p < 0.05$).

Migration from the site of implantation was determined for all tumour foci for each larva ($n > 20$/panel) and represented per group in scatter dot-plots (Figure 4C; see also supplementary material, Figure 6). Quantification of these plots by mean cumulative migration distance of tumour cell foci (MCD; see supplementary material, Figure S7) indicate that treatment with both Nutlin-3 and YK-4-279 reduced the number of tumour cell foci migrating from the site of implantation.

Our *in vivo* results substantiate our findings regarding growth in cultured cells with equal treatment times (see supplementary material, Figure S7), as well as previously described research on single treatments with these compounds on EWS cells [9,37]. Additionally, we managed to rapidly investigate the synergistic effects that these two compounds had on ES, showing an additive effect of combined treatment on the reduction of tumour burden *in vivo*.

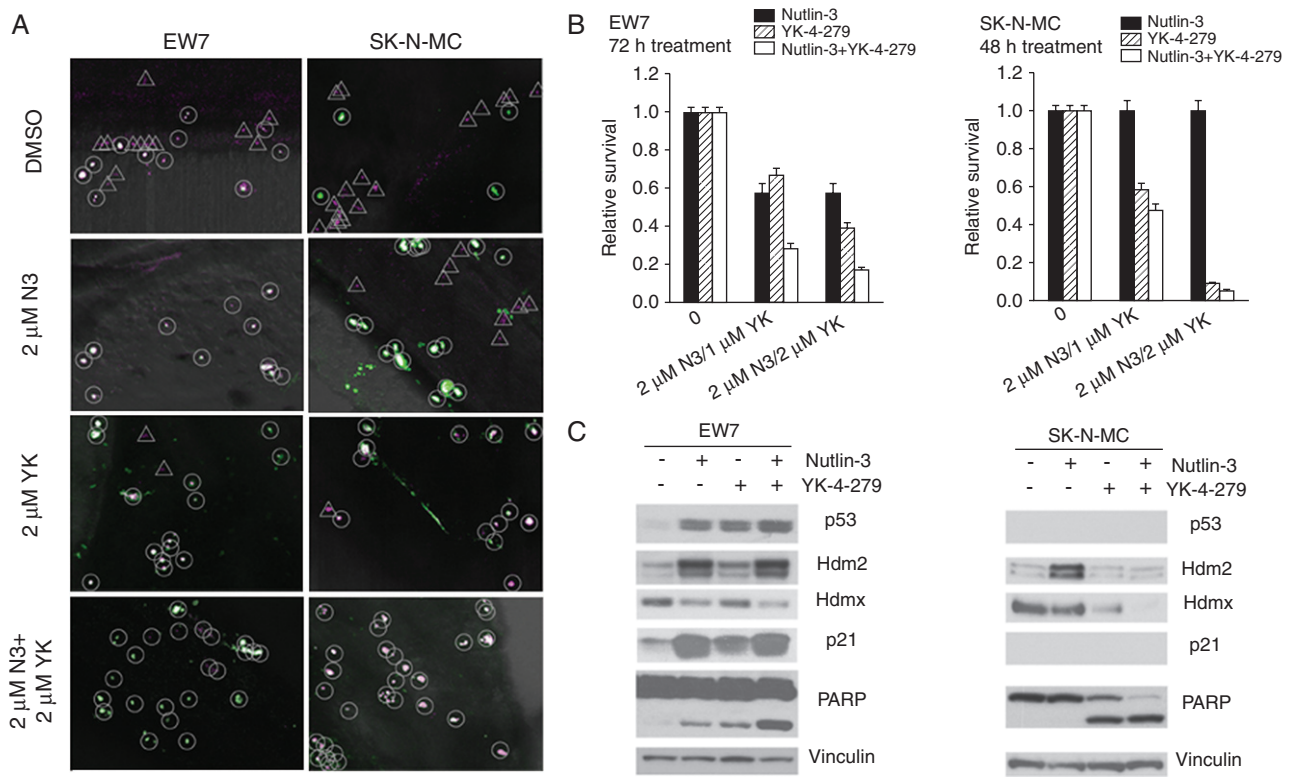

Figure 5. Apoptosis of EWS cells in 4 dpi wild-type embryos. (A) Whole-mount TUNEL staining of EWS cells in the muscle, fins or abdomen of ABTL embryo, 72 h after treatment. Apoptotic EWS cells are indicated by circles, non-apoptotic EWS cells by triangles. A certain amount of background apoptosis (<5%) was observed in all groups, independent of treatment (unmarked green cells). Data are representative images of three or more independent experiments (each $n > 25$). (B) The relative survival of EW7 and SK-N-MC cells treated with various concentrations of Nutlin-3 and YK-4-279 or a combination thereof, for 72 h (EW7) or 48 h (SK-N-MC), was determined by WST-1 assay, as described in Materials and methods. All measurements were performed in triplicate; error bars represent 95% confidence interval. (C) Western blot for EW7 and SK-N-MC cells treated for 72 h or 48 h, respectively, with 2 μM Nutlin-3, 2 μM YK-4-279 or a combination thereof. The earlier time point was chosen for SK-N-MC because 2 μM YK-4-279 caused such a high lethality in SK-N-MC cells after 72 h, making it impossible to harvest cells to make protein extracts

Induction of apoptosis by Nutlin-3 and YK-4-279 on EWS cells *in vivo* and in culture

To further assess the effect of Nutlin-3 and YK-4-279 on EW7 and SK-N-MC cells implanted in larvae, we performed whole-mount TUNEL staining to analyse the apoptotic response. DMSO-treated larvae revealed only a fraction of the grafted EWS cells undergoing apoptosis at 96 hpi (Figure 5A). Upon administration of Nutlin-3 on grafted embryos, the apoptotic response was increased more effectively in EW7 cells than in SK-N-MC cells (43.3 ± 15.7 to $71.0 \pm 8.2\%$ and 35.4 ± 8.3 to $40.8 \pm 11.5\%$, respectively), while both cell lines responded equally effectively to YK-4-279 treatment ($86.4 \pm 5.4\%$ for EW7 and $86.6 \pm 6.2\%$ for SK-N-MC). Treatment with both compounds simultaneously showed that the majority of cells underwent apoptosis in both EW7 ($92.0 \pm 6.4\%$) and SK-N-MC ($90.6 \pm 4.6\%$).

Protein analysis of cells treated in culture (Figure 5C; corresponding WST-1 proliferation assays for these conditions are found in Figure 5B) revealed that in EW7, both compounds increased p53 protein levels, p21 and cleaved PARP. This increase resembles the induction of cell-cycle arrest and apoptosis by both YK-4-279 and Nutlin-3. In SK-N-MC, full-length p53 and p21 are undetectable, but YK-4-279 could induce cleaved PARP, an apoptotic marker.

The data obtained both *in vivo* and in culture show that YK-4-279 induces apoptosis in EWS cells in a p53-independent manner, whilst apoptosis induced by Nutlin-3 is p53-dependent. Combined treatment increased apoptosis of tumour cells by engaging these mechanistically distinct pathways simultaneously.

Discussion

In this study, we investigated the additive effect of p53 reactivation on disruption of EWSR1–FLI1 transcriptional activity as a therapeutic strategy against Ewing sarcoma. EWS is a highly aggressive, malignant bone and soft-tissue tumour for which currently, when presented with metastatic spread, no satisfactory treatment regime has been developed. *TP53* is wild-type in ~90% of EWS cases [7] and up-regulation provides an attractive approach for intervention. EWS cells have been shown to lose viability upon forced wild-type p53 expression [42]. Alterations of *TP53* as well as *CDKN2A/CDKN2B* (p16), another important regulator

of G_1–S transition, are described to be correlated with an unfavourable prognosis [43–45].

We applied a newly-developed zebrafish ES-engraftment model to assess reactivation of p53 by Nutlin-3 as a treatment approach against these tumours. EWS cell lines implanted in zebrafish embryos could induce angiogenesis, migrate and proliferate within a week after implantation, mimicking the human situation in a model system. As the embryos can take up a range of compounds from the water, the zebrafish model allows rapid medium- to high-throughput screening of preclinical compounds in multiple subjects and can be a useful complement to established rodent models. Two practical matters need to be taken into account: the compounds need to be water-soluble and taken up by the embryo. Further, in the time frame of the experiment, embryonic cells are rapidly dividing and migrating, which might pose a problem, as these are features that many anti-cancer drugs are targeting. In treatment strategy design, we took into consideration that pathways that are important in cancer development can also be involved in organ-developmental processes. We observed less toxicity when compounds were applied at 3 dpf, when the larvae had already undergone some of the most crucial developmental processes. All compounds in the described experiments were tested for their toxicity; concentrations administered to engrafted embryos were chosen as high as possible to maximize the effect on EWS cells whilst still ensuring sufficient survival to perform analyses. The use of *tp53*^{M214K} mutant larvae, which fail to undergo apoptosis in response to γ-radiation, indicating aberrant p53 signalling [46], determined that Nutlin-3 worked specifically on EWS cells and not via host cells.

To inhibit EWS progression via inactivation of two essential tumourigenic mechanisms and investigate their therapeutic value *in vivo*, we applied Nutlin-3 and YK-4-279 to EWS cell engraftments in zebrafish. Nutlin-3 was used to stabilize p53 by blocking its interaction with MDM2, whilst YK-4-279 blocks interaction between RNA helicase A and EWS–FLI1 protein, deregulating gene transactivation and inducing apoptosis. EWS cells with a different *TP53* status were used, to show specificity of the reduction of tumour cell burden by these compounds *in vivo*. The tumour burden of both cell lines was significantly reduced by the addition of YK-4-279, while Nutlin-3 reduced tumour growth only of the *TP53* wild-type cells. Interestingly, although the tumour burden of *TP53*-deletion cells was not significantly affected by treatment with Nutlin-3, a slight induction of apoptosis *in vivo* was observed, suggesting a less straightforward response than found in culture data. Combinatory treatment had an additive effect on reduction of tumour burden of *TP53* wild-type cells by engaging distinct pathways of apoptosis, and confirmed that the model is applicable to study possible synergy between compounds.

In this model, treatments were applied relatively soon after implantation, to achieve the longest possible treatment time before additional immune systems become activated and engraftments may be rejected. As Ewing sarcoma patients often present with metastases at the time of diagnosis, any promising treatment found needs to be tested in a model where tumours are already established. Either immune-suppressed zebrafish or murine models should provide additional information before taking these compounds to clinical trials.

Several phase I clinical trials with RO5045337, an analogue of Nutlin-3 suitable for oral administration, have been completed. Currently, a follow-up trial is active for various cancer types, amongst which are patients presenting with soft tissue sarcoma (NCT01677780). Additionally, clinical trails with other HDM2 antagonists are also ongoing (NCT01877382, NCT01462175) [47] and could perform a similar synergistic function as Nutlin-3. A racemic mixture of YK-4-279 was used for all tests performed in this study. Recent investigations show that the (S)-YK-4-279 enantiomer has enhanced therapeutic potency compared to a mixture of this compound [48]. This increased specificity could minimize off-target effects and brings this compound one step further to the initiation of clinical trials.

In conclusion, using the high-throughput zebrafish model, we found that simultaneous induction of the p53 pathway and disruption of EWS–FLI1 transcriptional activity had an additive effect on the reduction of EWS malignancy *in vivo*. Combining different treatment strategies with reactivation of the p53 pathway in this tumour type may be a promising therapeutic strategy for the subset of EWS patients harbouring wild-type *TP53*, and should be investigated in further detail in murine models before initiating clinical trials.

Acknowledgements

The authors are grateful to Frans Prins for assistance with histology, Hans de Bont for assistance with confocal image analysis and Rubén Marín-Juez for critical reading of the manuscript. This study was supported by Stichting Kinderen Kankervrij (Grant No. 30677).

Author contributions

WE and AGJ designed and performed experiments, analysed and interpreted data and wrote the paper; AFAST performed experiments and analysed and interpreted data; SFGK performed experiments, interpreted data and wrote the paper; and KS, HPS, PCWH and BESJ designed experiments, interpreted data and wrote the paper.

References

1. Fletcher CDM, Bridge JA, Hogendoorn PCW, *et al. WHO Classification of Tumours of Soft Tissue and Bone*, 4th edn. IARC: Lyon, 2013.

2. Burchill SA. Molecular abnormalities in Ewing's sarcoma. *Expert Rev Anticancer Ther* 2008; **8:** 1675–1687.
3. Delattre O, Zucman J, Plougastel B, *et al.* Gene fusion with an ETS DNA-binding domain caused by chromosome translocation in human tumours. *Nature* 1992; **359:** 162–165.
4. Sorensen PH, Lessnick SL, Lopez-Terrada D, *et al.* A second Ewing's sarcoma translocation, t(21;22), fuses the *EWS* gene to another ETS-family transcription factor, *ERG*. *Nat genet* 1994; **6:** 146–151.
5. Verhoeven DH, de Hooge AS, Mooiman EC, *et al.* NK cells recognize and lyse Ewing sarcoma cells through NKG2D and DNAM-1 receptor dependent pathways. *Mol Immunol* 2008; **45:** 3917–3925.
6. Balamuth NJ, Womer RB. Ewing's sarcoma. *Lancet Oncol* 2010; **11:** 184–192.
7. Neilsen PM, Pishas KI, Callen DF, *et al.* Targeting the p53 pathway in Ewing sarcoma. *Sarcoma* 2011; **2011:** 746939.
8. Vassilev LT, Vu BT, Graves B, *et al. In vivo* activation of the p53 pathway by small-molecule antagonists of MDM2. *Science* 2004; **303:** 844–848.
9. Erkizan HV, Kong Y, Merchant M, *et al.* A small molecule blocking oncogenic protein EWS–FLI1 interaction with RNA helicase A inhibits growth of Ewing's sarcoma. *Nat Med* 2009; **15:** 750–756.
10. Sonnemann J, Palani CD, Wittig S, *et al.* Anticancer effects of the p53 activator nutlin-3 in Ewing's sarcoma cells. *Eur J Cancer* 2011; **47:** 1432–1441.
11. Liu S, Leach SD. Zebrafish models for cancer. *Annu Rev Pathol* 2011; **6:** 71–93.
12. Goessling W, North TE, Zon LI. New waves of discovery: modeling cancer in zebrafish. *J Clin Oncol* 2007; **25:** 2473–2479.
13. Ung CY, Lam SH, Gong Z. Comparative transcriptome analyses revealed conserved biological and transcription factor target modules between the zebrafish and human tumors. *Zebrafish* 2009; **6:** 425–431.
14. Feitsma H, Cuppen E. Zebrafish as a cancer model. *Mol Cancer Res* 2008; **6:** 685–694.
15. Amatruda JF, Shepard JL, Stern HM, *et al.* Zebrafish as a cancer model system. *Cancer Cell* 2002; **1:** 229–231.
16. Lam SH, Chua HL, Gong Z, *et al.* Development and maturation of the immune system in zebrafish, *Danio rerio*: a gene expression profiling, *in situ* hybridization and immunological study. *Dev Comp Immunol* 2004; **28:** 9–28.
17. Goessling W, North TE, Zon LI. New waves of discovery: modeling cancer in zebrafish. *J Clin Oncol* 2007; **25:** 2473–2479.
18. Kari G, Rodeck U, Dicker AP. Zebrafish: an emerging model system for human disease and drug discovery. *Clin Pharmacol Ther* 2007; **82:** 70–80.
19. den Hertog J. Chemical genetics: drug screens in zebrafish. *Biosci Rep* 2005; **25:** 289–297.
20. Zon LI, Peterson RT. *In vivo* drug discovery in the zebrafish. *Nat Rev Drug Discov* 2005; **4:** 35–44.
21. Parng C, Seng WL, Semino C, *et al.* Zebrafish: a preclinical model for drug screening. *Assay Drug Dev Technol* 2002; **1:** 41–48.
22. Lawson ND, Weinstein BM. In vivo imaging of embryonic vascular development using transgenic zebrafish. *Dev Biol* 2002; **248:** 307–318.
23. Renshaw SA, Loynes CA, Trushell DM, *et al.* A transgenic zebrafish model of neutrophilic inflammation. *Blood* 2006; **108:** 3976–3978.
24. Langenau DM, Feng H, Berghmans S, *et al.* Cre/lox-regulated transgenic zebrafish model with conditional myc-induced T cell acute lymphoblastic leukemia. *Proc Natl Acad Sci USA* 2005; **102:** 6068–6073.
25. Ghotra VP, He S, de Bont H, *et al.* Automated whole animal bio-imaging assay for human cancer dissemination. *PloS One* 2012; **7:** e31281.
26. Chou TC. Theoretical basis, experimental design, and computerized simulation of synergism and antagonism in drug combination studies. *Pharmacol Rev* 2006; **58:** 621–681.
27. Lam S, Lodder K, Teunisse AF, *et al.* Role of Mdm4 in drug sensitivity of breast cancer cells. *Oncogene* 2010; **29:** 2415–2426.
28. Krens SF, He S, Lamers GE, *et al.* Distinct functions for ERK1 and ERK2 in cell migration processes during zebrafish gastrulation. *Dev Biol* 2008; **319:** 370–383.
29. Forbes SA, Tang G, Bindal N, *et al.* COSMIC (the Catalogue of Somatic Mutations in Cancer): a resource to investigate acquired mutations in human cancer. *Nucleic Acids Res* 2010; **38:** D652–657.
30. Szuhai K, Ijszenga M, Tanke HJ, *et al.* Molecular cytogenetic characterization of four previously established and two newly established Ewing sarcoma cell lines. *Cancer Genet Cytogenet* 2006; **166:** 173–179.
31. Moll UM, Ostermeyer AG, Haladay R, *et al.* Cytoplasmic sequestration of wild-type p53 protein impairs the G_1 checkpoint after DNA damage. *Mol Cell Biol* 1996; **16:** 1126–1137.
32. Ottaviano L, Schaefer KL, Gajewski M, *et al.* Molecular characterization of commonly used cell lines for bone tumor research: a trans-European EuroBoNet effort. *Genes Chromosomes Cancer* 2010; **49:** 40–51.
33. Whang-Peng J, Triche TJ, Knutsen T, *et al.* Cytogenetic characterization of selected small round cell tumors of childhood. *Cancer Genet Cytogenet* 1986; **21:** 185–208.
34. Nicoli S, Presta M. The zebrafish/tumor xenograft angiogenesis assay. *Nat Protoc* 2007; **2:** 2918–2923.
35. Nicoli S, Ribatti D, Cotelli F, *et al.* Mammalian tumor xenografts induce neovascularization in zebrafish embryos. *Cancer Res* 2007; **67:** 2927–2931.
36. White RM, Sessa A, Burke C, *et al.* Transparent adult zebrafish as a tool for *in vivo* transplantation analysis. *Cell Stem Cell* 2008; **2:** 183–189.
37. Pishas KI, Al-Ejeh F, Zinonos I, *et al.* Nutlin-3a is a potential therapeutic for Ewing sarcoma. *Clin Cancer Res* 2011; **17:** 494–504.
38. Stern HM, Zon LI. Cancer genetics and drug discovery in the zebrafish. *Nat Rev Cancer* 2003; **3:** 533–539.
39. Peirce SK, Findley HW. The MDM2 antagonist nutlin-3 sensitizes *p53*-null neuroblastoma cells to doxorubicin via E2F1 and TAp73. *Int J Oncol* 2009; **34:** 1395–1402.
40. Ray RM, Bhattacharya S, Johnson LR. Mdm2 inhibition induces apoptosis in p53-deficient human colon cancer cells by activating p73- and E2F1-mediated expression of PUMA and Siva-1. *Apoptosis* 2011; **16:** 35–44.
41. Rentzsch F, Kramer C, Hammerschmidt M. Specific and conserved roles of TAp73 during zebrafish development. *Gene* 2003; **323:** 19–30.
42. Kovar H, Pospisilova S, Jug G, *et al.* Response of Ewing tumor cells to forced and activated p53 expression. *Oncogene* 2003; **22:** 3193–3204.
43. Wei G, Antonescu CR, de Alava E, *et al.* Prognostic impact of INK4A deletion in Ewing sarcoma. *Cancer* 2000; **89:** 793–799.
44. Lopez-Guerrero JA, Pellin A, Noguera R, *et al.* Molecular analysis of the 9p21 locus and p53 genes in Ewing family tumors. *Lab Invest* 2001; **81:** 803–814.
45. Huang HY, Illei PB, Zhao Z, *et al.* Ewing sarcomas with *p53* mutation or p16/p14ARF homozygous deletion: a highly lethal subset associated with poor chemoresponse. *J Clin Oncol* 2005; **23:** 548–558.
46. Berghmans S, Murphey RD, Wienholds E, *et al. tp53* mutant zebrafish develop malignant peripheral nerve sheath tumors. *Proc Natl Acad Sci USA* 2005; **102:** 407–412.

47. Ji Z, Kumar R, Taylor M, *et al.* Vemurafenib synergizes with nutlin-3 to deplete survivin and suppresses melanoma viability and tumor growth. *Clin Cancer Res* 2013; **19:** 4383–4391.

48. Barber-Rotenberg JS, Selvanathan SP, Kong Y, *et al.* Single enantiomer of YK-4–279 demonstrates specificity in targeting the oncogene EWS–FLI1. *Oncotarget* 2012; **3:** 172–182.

SUPPLEMENTARY MATERIAL ON THE INTERNET

The following supplementary material may be found in the online version of this article:

Figure S1. Angiogenesis controls

Figure S2. High-resolution histology images of five dpi embryos with CD-99 positive EWS cells

Figure S3. Implantation in bloodstream of 35 dpf zebrafish juveniles with EWS cells

Figure S4. In-culture effect of Nutlin-3 and YK-4-279 on TC32 and CADO-ES1.WST-1 assay for measuring relative survival of CADO-ES1 or TC32 cellstreated for 72 h with Nutlin-3, YK-4-279 or a combination thereof

Figure S5. Zebrafish survival curves

Figure S6. Quantification of migration of EWS cells in zebrafish

Figure S7. In-culture effect of Nutlin-3 and YK-4-279 on EWS cells for prolonged exposure